DETECTION OF WEAK SEISMIC SIGNALS IN NOISY ENVIRONMENTS FROM UNFILTERED, CONTINUOUS PASSIVE SEISMIC RECORDINGS

M. Kinali[1*], S. Pytharouli[1], R.J. Lunn[1], Z. K. Shipton[1], M. Stillings[1], R. Lord[1] and S. Thompson[2]

[1]University of Strathclyde, Department of Civil and Environmental Engineering, University of Strathclyde, Glasgow, James Weir Building, Level 5, 75 Montrose Street, Glasgow, G1 1XJ, United Kingdom

[2]Radioactive Waste Management, Building 587 , Curie Avenue, Harwell Oxford, Didcot, Oxfordshire, OX11 0RH, United Kingdom

* Corresponding author: Marianna Kinali, email: marianna.kinali@strath.ac.uk

A peer-reviewed, accepted author manuscript of the following research article: Kinali, M., Pytharouli, S., Lunn, R., Shipton, Z., Stillings, M., Lord, R., & Thompson, S. (2018). Detection of weak seismic signals in noisy environments from unfiltered, continuous passive seismic recordings. Bulletin of the Seismological Society of America.

ABSTRACT

Robust event detection of low signal-to-noise ratio (SNR) events, such as those characterized as induced or triggered seismicity, remains a challenge. The reason is the relatively small magnitude of the events (usually less than 2 or 3 in Richter scale) and the fact that regional permanent seismic networks can only record the strongest events of a microseismic sequence. Monitoring using temporary installed short-period arrays can fill the gap of missed seismicity but the challenge of detecting weak events in long, continuous records is still present. Further, for low SNR recordings, commonly applied detection algorithms generally require pre-filtering of the data based on a priori knowledge of the background noise. Such knowledge is often not available.

We present the NpD (Non-parametric Detection) algorithm, an automated algorithm which detects potential events without the requirement for pre-filtering. Events are detected by calculating the energy contained within small individual time segments of a recording and comparing it to the energy contained within a longer surrounding time window. If the excess energy exceeds a given threshold criterion, which is determined dynamically based on the background noise for that window, then an event is detected. For each time window, to characterize background noise the algorithm uses non-parametric statistics to describe the upper bound of the spectral amplitude. Our approach does not require an assumption of normality within the recordings and hence it is applicable to all datasets.

We compare our NpD algorithm with the commonly commercially applied STA/LTA algorithm and another highly efficient algorithm based on Power Spectral Density using a challenging microseismic dataset with poor SNR. For event detection, the NpD algorithm significantly outperforms the STA/LTA and PSD algorithms tested, maximizing the number of detected events whilst minimizing the number of false positives.

INTRODUCTION

Microseismic monitoring refers to the recording and detection of small in magnitude (less than M_L 3) earthquakes. It was mainly developed in the framework of the Test Ban Treaty (late 1950s) for the monitoring of the relaxation of the rock mass after nuclear weapon testing (Lee and Stewart, 1981). In such a demanding environment, microseismic monitoring proved to be a powerful tool, tuned to detect weak seismic signals in low signal-to-noise ratios. Induced (RIS) or Triggered Seismicity (RTS) mainly consists of sequences of microearthquakes with magnitudes M_L 3 or less. Unless there are specific concerns of the occurrence of RIS/RTS, the phenomenon is usually monitored by existing national seismic networks with completeness magnitudes usually down to M = 2 or 1. Microseismic monitoring based on temporary installations has the potential to provide missed information on the occurrence of shocks with magnitudes M_L=0 or even less than that (e.g. Pytharouli et al. (2011)). Hence, its applications have expanded into a wide range of projects related to RIS/RTS including the monitoring of rockslides and landslides (Helmstetter et al. (2010); Torgoev et al. (2013); Yfantis et al. (2014)), the monitoring of fracking processes (Maxwell (2011)), reservoir monitoring for geological CO_2 (Zhou (2010)) and radioactive waste disposal (Young et al. (1993)). A microseismic monitoring configuration mainly consists of short-period seismic arrays, with the components (seismometers) placed in a grid or triangular geometry, depending on their number. For short-duration projects and temporary installations, one array consisting of four (single or three-component) seismometers, deployed in a triangular geometry, is regarded adequate (Joswig (1992)).

59 The high sensitivity of a microseismic monitoring system is also its main caveat. Seismometers
60 record every vibration of the ground that is caused by any type of sources, at distances that can
61 extend to tens of kilometers depending on the site conditions and the energy emitted by the seismic
62 source. In addition, instrumental self-noise is present at all times. As a result, it can be extremely
63 difficult to distinguish between the microseismicity that is of interest to a project and everything
64 else. Such circumstances may be less problematic for projects such as hydro-fracturing, where the
65 likely location and time of occurrence of microseismicity is known a priori. But for the vast
66 majority of applications, this is not the case and peaks in ambient noise can be mistakenly regarded
67 as microseismic events. A false increase in the recorded frequency of microseismic events will
68 bias project results. Furthermore, manual verification of each event will result in significant data
69 processing time, yet neglecting verification can lead to other adverse economic impacts; for
70 example, unnecessary road closures due to the false triggering of an early warning system for
71 landslides. By contrast, relaxing event detection criteria to avoid false alarms can result in excess
72 risk, with microseismic events remaining undetected. Monitoring for longer than a couple of days
73 and with a sampling rate between 200 – 250 Hz (a range adequate for the needs of most projects
74 requiring microseismic monitoring) leads to vast datasets that are not cost effective for visual
75 inspection and require a computational detection approach.

76 A number of automatic detection approaches have been developed that work in the time or
77 frequency domain or both e.g., Freiberger (1963); Goforth and Herrin (1981); Joswig (1990);
78 Gibbons and Ringdal (2006); Küperkoch et al. (2010); Vaezi and Van de Baan (2014), to name a
79 few. For a more detailed review on existing detection algorithms see Supplementary material,
80 Section A.

All detection algorithms have advantages and shortcomings with no algorithm being clearly optimal under all source, receiver, path and noise conditions (Withers et al. (1998)). The most widely used event detection algorithm at present is the STA/LTA (Bormann (2012)) which operates in the time-domain. STA/LTA is an excellent onset time detector for adequately high SNR events; a condition that may not be true in the case of weak microseismic events. Also, the method can lead to false triggers unless the data used are optimally filtered to minimize the effect of noise; this is difficult to achieve in a varying noise background. In fact, in all algorithms where bandpass filtering is part of the detection process (STA/LTA or Goforth's and Herrin's algorithm), some kind of a priori knowledge on the expected signals is assumed. The choice of the filter to be used is important, as inappropriate filtering can result in the removal of useful information from the data.

The method by Vaezi and Van de Baan (2014) was found to outperform the STA/LTA technique by detecting a higher number of weak events while keeping the number of false alarms at a reasonable level (Vaezi and Van de Baan (2015)). It requires, however, some pre-processing where all noise bursts or transients that may exist in the data are removed. It also assumes stationary noise that follows a normal distribution and, therefore, employs the mean and standard deviation as statistical tools. Although this might be a good approximation for recordings with high SNR, it is not the case for seismic data with low SNR. In such cases, the average PSD is not representative of the central tendency of noise and as such any detection criteria based on deviation from the mean could lead to a large number of 'false' detections. This is particularly important where long, continuous recordings are available as it can significantly increase the processing time and bias the results.

The aim of this paper is twofold: first, we present a methodology for the characterization of the background noise in microseismic recordings. This is an important step in the analysis as it allows for the characteristics of noise to be revealed, i.e. whether it is a stationary or non-stationary process, and helps making informed decisions on the value of parameters in subsequent analyses for automatic event detection. Second, we propose a new detection algorithm, namely NpD (Non-parametric detection) algorithm, which assumes the presence of non-stationary noise and most importantly, does not require any bandpass filtering of the microseismic records. The algorithm operates in the frequency domain, using the Power Spectral Density (Welch (1967)) and it has been implemented in Matlab. The NpD algorithm is influenced by the research of Shensa (1977) and Vaezi and van der Baan (2014). We extend their method by introducing non-parametric statistics and a dynamic event detection threshold, to be applicable to datasets with non-stationary background noise.

THE POWER SPECTRAL DENSITY (PSD) SPECTRUM

The Power Spectral Density (PSD) spectrum can be estimated using Fourier transforms, such as the Welch's modified periodogram method (1967) or other techniques such as the maximum entropy method (Kesler (1978)). The PSD of a signal refers to the spectral energy distribution per unit time and is simply the representation of the signal in the frequency domain (Press et al. (2007)), measured in squared magnitude units of the time series data per unit frequency.

Background noise and microseismic event discrimination based on the PSD spectrum

Microseismic events have been found to represent stronger spectral content over a frequency band that depends on the nature of the event, than that of background noise (Vaezi and van der Baan (2014)). According to this, a microseismic event can be regarded as an outlier, i.e. a data value or values that are outwith an expected range which represents the noise. The challenge is to define the upper bound of this range when no a priori knowledge of the expected signal (in terms of amplitude and frequency content) is available.

In statistical analyses, for populations that are normally distributed, the detection of outliers is usually based on the 3σ criterion, where σ is the standard deviation of the data (Barnett et al. (1994)). Any values that are outwith the $\pm 3\sigma$ range are considered outliers. This range includes 99.7% of the data. For populations that are not normally distributed though, this criterion could lead to erroneous results as the mean is not necessarily the best quantity to describe the central tendency of the data. Even if the PSD values are indeed normally distributed for one hour of data, it does not guarantee that this will be the case for the full duration of the data set. A robust method for the characterization of the background noise and the determination of an upper bound for the noise PSD value is required.

SPECTRAL CHARACTERISATION OF BACKGROUND NOISE

Background seismic noise can result from numerous sources: natural perturbations, e.g. tides, tectonics, seasonal changes, etc., and man-made perturbations. Perturbations can have a periodic or transient nature; their durations may differ from instantaneous bursts to elevated noise that lasts for hours, days or even months; in the case of seismic arrays, noise amplitudes may vary between

147 seismometers at different locations. Investigations of the seismic noise in hydrofracking sites have
148 shown that noise has nonstationary properties, correlated in both time and space (e.g. Chambers et
149 al. (2010)). Despite this, most detection algorithms assume normality for the noise distribution
150 (e.g., Vaezi and Van der Baan (2014) and (2015)).

151 The following methodology allows for the determination of a characteristic level of background
152 noise in the frequency domain through examination of the statistical distribution of its PSD
153 spectrum. Knowing the distribution allows for the determination of the appropriate statistics, i.e.
154 parametric or non-parametric, to be used in further analysis.

155

156 **Characteristic spectral level of background noise (Noise PSD)**

157 To determine a characteristic upper bound to the spectral amplitude of background noise, from
158 here onwards named Noise PSD, over hourly, daily, or any other duration, time periods (temporal
159 variation) and at seismometers deployed at different locations (spatial variation) we introduce a
160 methodology based on the power spectral density (PSD).

161 We compute the individual PSDs for N_w non-overlapping (to ensure that the data between
162 segments are statistically independent) segments of duration t_l for the frequency range 0 - Nyquist
163 frequency, f_{Nyq} using the Welch's modified method (Welch (1967)); see also Supplementary
164 material, Section B). The PSD is calculated at discrete frequencies within this range. The total
165 duration of the data set is then $N_w * t_l$. In general, the duration of an individual segment should
166 include at least two full cycles of the expected signal. We suggest a duration of 0.5 to 2 seconds is
167 adequate for microseismicity due to shear failure. For research on other types of microseismic

events, such as those induced during a landslide, segments with longer durations are recommended.

Upon completion of the PSD calculations for each individual segment, there are N_w PSD values for each discrete frequency in the range 0 - f_{Nyq}. To determine normality in the PSD values for a specific frequency, graphical methods, i.e. histograms, probability plots and boxplots, can be used. An alternative to graphical methods are normality tests such as Shapiro-Wilk test S-W (Razali (2011)) and Kolmogorov-Smirnov K-S test (Massey (1951)).

If the normality check results in normally distributed PSD values for each frequency of the PSD spectrum, then a mean PSD value and a standard deviation (σ) for each specific frequency can be calculated. The Noise PSD (i.e. the characteristic upper bound) value for each individual frequency can then be specified by applying the $\pm 3\sigma$ criterion or any other suitable combination between the mean and the standard deviation as an upper threshold, e.g. mean $\pm \sigma$.

If the normality testing reveals a non-normal distribution, an upper bound for the background noise can be determined using non-parametric statistics, i.e. percentiles. We recommend that a high percentile, between 75 and 90, is chosen. The Noise PSD is then defined by the chosen percentile PSD value at each discrete frequency f.

THE NpD EVENT DETECTION ALGORITHM

The NpD event detection algorithm (Non-parametric detection) enables microseismic events to be discriminated without any prior filtering of the data.

The algorithm is an alternative detection approach for data sets with low signal-to-noise ratios. It is based in the frequency domain by searching and detecting any changes in the PSD spectrum of the data recordings compared to the Noise PSD.

The algorithm is described on the basis of continuous recordings $x(t)$ of any duration, though 1-hour durations provide computational and time efficiency. The algorithm is executed in two Steps in order to minimize the computational time required. At the first step, (Step 1) a scan is performed to identify time segments that could potentially contain a microseismic event (or any other signal of interest in the more general case). Only those time segments that are picked in Step 1 are further investigated to detect potential microseismicity, or rejected altogether. The procedure is described in detail below:

Step 1- Calculation of the excess energy over a continuous data record

Following the background noise spectral characterization methodology described in the previous section, the Noise PSD for each data record $x(t)$ is calculated. The individual time segment duration t_l to which the data record is divided, is chosen large enough to be able to accommodate the energy of a microseismic event or a representative energy section of a long-period long-duration event (Das and Zoback (2011)) whilst at the same time small enough to be able to pick closely-spaced events. It is not necessary for the NpD algorithm to include full cycles of the expected signal.

Next, the Noise PSD is subtracted from the PSD of each individual time segment forming a set of differences. Within each one of the N_w individual time segments, only the positive differences are

kept and summed. This sum is termed *excess energy* which, for each individual time segment starting at time t, is given by:

$$PSD\_excess_n^t = \begin{cases} \sum_{f=0}^{Nyq}(PSD_n^t(f) - Noise\ PSD(f)), & if\ PSD_n^t(f) - Noise\ PSD(f) > 0 \\ 0, & otherwise \end{cases}, \quad \text{(eq. 1)}$$

where $n = 1,2,..,N_w$

The total number of non-zero only, excess energy values, described here as N_1, is equal to or less than the number N_w of the individual time segments that the data record is split to. The results of this process can be graphically presented as a scatterplot with each point's coordinates being pairs of ($PSD\_excess_n^t$, t), with t being the start time of the n^{th} individual time segment.

Excess energy threshold determination

Not all N_1 excess energy values are accepted. In data records with highly variable background noise, the detection procedure described so far might result in a number of incorrect detections that do not correspond to events. In order to minimize this possibility, we introduce a threshold value and only accept those ($PSD\_excess_n^t$, t) pairs for which the excess energy is above this threshold.

The threshold is determined based on the statistical properties of the excess energy values over the duration of the data record analyzed; more specifically, the first (Q1) and third quartiles (Q3) of the excess energy values. We then define the threshold value as:

$$Threshold = Q3 + 0.5 \times IQR, \quad \text{(eq. 2)}$$

where $IQR = Q3 - Q1$.

For the detection of outliers using the quartile values, a commonly used threshold is given by Q3 + 1.5×IQR, with the 1.5 factor justified by the standard normal distribution and leading to a probability of 99.3% for correctly detecting no outliers (Sun and Genton (2012)). We adopt the value 0.5 as a more conservative threshold.

Only N_2 (out of the total N_1) excess energy values are eventually above the threshold and these are processed in the next Step of the analysis (Step 2). This reduces the calculation time significantly.

Step 2 - Calculation of the excess energy over a local time window

Step 2 is exactly the same as Step 1, but now the Noise PSD refers to a local time window rather than the duration of the full data record $x(t)$. This local time window, has a predetermined length and is centered around the starting time t of each of the N_2 individual time segments that fulfilled the criteria of Step 1. The total number of local time windows used in Step 2 is N_2 and as a result the methodology of Step 1 is repeated N_2 times in Step 2: A Noise PSD and then the excess energy and threshold are calculated for each one of the N_2 local time windows as described previously.

The times corresponding to the excess energy values that are higher than the threshold for each of the local time windows in Step 2 constitute the approximate times where a potential event occurred.

Detected events: Microseismicity or local noise?

A detected potential event from Step 2 could still represent local noise, e.g. steps, drilling noise or even an instrumental glitch. This possibility can be minimized by combining the NpD results from multiple seismometers, for example, from a whole array (voting scheme, Trnkoczy (1999)). A real

250 microseismic event, irrespectively of how small it is, should be recorded by neighboring
251 seismometers. This is not the case for a local noise burst that is usually recorded by the
252 seismometer closest to it, nor for a mechanical glitch.

253 The number of seismometers that are required to have recorded the same event depends on the
254 application and the distance between them. A time delay between seismometers for the same event
255 should also be considered.

256 To avoid having multiple true positives (i.e. correctly identified events) corresponding to different
257 phases of the same event (i.e. different peaks in the same microseismic waveform), we decided to
258 'clean-up' consecutive events that are detected in consecutive PSD time segments. Consequently,
259 only the first arrival from the consecutives is considered a trigger. This decision was verified
260 during a sensitivity analysis for several hours of data, to ensure that it does not result in missed
261 true positives.
262

CASE STUDY: DETECTION OF MICROSEISMICITY AT GRIMSEL TEST SITE (GTS) USING THE NpD ALGORITHM

Passive seismic monitoring at Grimsel Test Site

Microseismic monitoring was conducted as a part of the LASMO project (Nagra (2017)), to determine whether drainage and subsequent natural refilling of Lake Raeterichsboden can be associated with hydro-mechanical changes within the surrounding rock mass. LASMO aims to evaluate existing monitoring techniques in a repository-like environment. For a 30-month period, two short-period surface arrays were deployed at GTS as part of the microseismic monitoring network. Each array consisted of one three-component seismometer (LE3D-lite MKII) and three one-component sensors (LE1D-lite). Seismometers within an array were deployed at approximately 45 m distance from each other, and the two arrays were approximately 1.1 km apart. The arrays were deployed at the neighboring, to GTS, Gerstenegg tunnel, located in the Swiss Alps adjacent to Lake Raeterichsboden (Figure 1).

Passive seismic monitoring data

Data acquisition at GTS was initiated in November 2014 and lasted until June 2017. The sampling rate was 250Hz. The acquisition was continuous and data were stored in 1-hour long data files. Two full drainage and refilling cycles of the Lake Raeterichsboden took place during that period.

There are a large number of activities that contribute to seismic noise in the region; engineering activities within the GTS (drilling, hammering etc.), engineering activities in the surrounding tunnels, pumping and hydropower generation, tunnel boring, drilling, maintenance, and finally, natural background seismic noise such as glacial movement.

In order to explore the temporal and spatial variation of the spectral characteristics of the background noise at Grimsel test site, we followed the methodology for the background noise characterization described earlier. First, we determined whether the background noise followed a normal distribution in order to choose appropriate statistics and then checked if there were significant temporal or spatial variations in background noise.

To determine appropriate statistics for the analysis we needed to assess the assumption of normality for the distributions of all PSD values for the frequencies within the interval 0 – 125 Hz. We computed the PSDs, for all non-overlapping 2 second time windows within quiet hours at the frequency range (0-125 Hz). Hours outside of the GTS working hours, during which no tectonic events were reported by the Swiss Seismological Service catalogue (see Data and Resources Section), were randomly chosen to be used for this analysis. To determine if random samples of independent PSD observations were normally distributed, different graphical methods (histograms, probability plots and boxplots) and the Shapiro-Wilk test S-W (Razali (2011)) and Kolmogorov-Smirnov K-S test (Massey (1951)), were applied. Here we present indicatively, random hours within 04/11/2014 and 16/05/2015. Both S-W and K-S tests rejected the null hypothesis of normality in all cases checked ($p<0.05$). In fact, the noise PSD histograms are negatively skewed with positive kurtosis; examples for the frequencies of 30 and 85 Hz for the vertical component of the 3-component sensor in the North and of the South Array, located approximately 1km apart, are presented in Figure 2a and 2b respectively. The histograms are clearly not derived from normally distributed data, hence non-parametric statistics for noise characterization are appropriate. Also, the histograms for each sensor are different, hence background noise at each sensor is not the same. Figure 2a and 2b also show the two Noise PSDs derived for the same hour, using a characteristic upper bound of the 75th percentile. The value of

the 75th percentile for each frequency and how this is related to the noise PSD is clearly annotated on the Figure.

Further analysis (see Supplementary material, Section C) of the background noise demonstrated extremely large, highly unpredictable variations in background noise both between sensors and between consecutive hours/days on a single sensor. No repeatable pattern could be determined.

Application of the NpD algorithm for the detection of microseismicity at GTS

Three hours of microseismic data recordings from the North array over two consecutive days were chosen to test the sensitivity of the algorithm to two input parameters: the percentile used for the calculations of the Noise PSD (Step 1) and the length of the Local time window (in Step 2). More specifically, the following hours were selected and used: Hour 1: 15/03/2016 18:00 - 19:00 (UTC); Hour 2: 15/03/2016 19:00 - 20:00 (UTC); and Hour 3: 16/03/2016 05:00 - 06:00 (UTC).

Hours 1 and 2 were chosen because after visual inspection were found to contain a number of potential microseismic events. Hour 3 was chosen as a 'quiet hour' with no events visually confirmed. We located a random selection of the visually observed events to confirm that they are indeed events occurring in the surrounding area (within 8 km from the arrays). Three of them were subsequently found in the Swiss Seismological Service catalogue (see Data and Resources Section), having magnitudes down to M_L -0.6.

The visual inspection took place prior to applying the NpD algorithm. For the visual inspection, a bandstop, bidirectional two-pole Butterworth filter was applied to all Hours to remove the AC effect (the arrays were connected to the mains for power supply), as well as a high-pass 2 Hz filter

to suppress ambient noise. This was only done for the purpose of visually picking potential events. For the NpD algorithm we used raw data.

Figures 3-4 show plots of the filtered waveforms of Hours 1 and 2. The vertical lines above the waveforms indicate the visually observed events that are expected to be detected by the algorithm. We then applied the NpD algorithm for various combinations of percentiles within the range 75 – 95 (for the calculation of the Noise PSD) and local time window lengths. Tables 1 and 2 show the best outputs from the sensitivity analyses for these two hours, for each of the arrays individually. The number of the visually observed events is represented by the *Actual no of events* parameter. The number of events that each algorithm detects is represented by the *Detected events* parameter. Those events amongst the detected events that are also within the actual no of events, i.e. visually observed, are the *True positives*. The ratios $R1 = \frac{true\ positives}{detected}\ events \cdot 100\%$ and $R2 = \frac{true\ positives}{actual\ no\ of}\ events \cdot 100\%$ were formed to investigate the efficiency of the various combinations of parameters. Ratios R1 and R2 were introduced to quantify the tendency of the algorithm to trigger false positives, e.g. noise mistakenly picked as an event, and their detection efficiency, respectively. R1 and R2 take values between 0 and 100%. A high value for R1 would indicate a small amount of false positives, while for R2, a high value indicates high detection capability. Using these ratios the most efficient combination of parameters was chosen to be the one for which both R2 and R1 are at their highest values.

As shown in Table 1 and 2, all {percentile, local time window} combinations yield quite high R2 ratios (>84%), depending on the location and hour. The differentiating factor is the R1 ratio. Upon checking other combinations of parameters from the two Tables we also see that the R1, R2 ratios do not vary drastically within a particular hour and array. This means that the assumption that we

351 can treat seismic events as outliers and our choice of a dynamic threshold which adapts well to the
352 statistical properties of each examined segment work well. In the case Hour 3 (Figure 4), the hour
353 for which no visually observed events existed, the low number of events that the algorithm detected
354 was acceptable (Table 3).

355 For our project, the combination of parameters that best suited our data for identifying as many
356 seismic events with the least possible false positives was the 75^{th} percentile for the calculation of
357 the Noise PSD (Step 1) and a 300 second duration for the local time window (Step 2 of the NpD
358 algorithm).
359

360

361 **DISCUSSION**

362 **Main advantages of the NpD algorithm**

363 In this paper we presented a new algorithm for the detection of microseismic events at
364 environments with low SNR. The main advantage of our approach is that it does not require any
365 pre-filtering of the data as would be the case for detection of weak signals with most other
366 methodologies. Pre-filtering assumes a priori knowledge of the expected microseismic signals
367 which is seldom the case for passive monitoring applications. As a result, pre-filtering could
368 remove information from the recordings, discarding it as noise, especially in cases of low SNR
369 data. Avoiding pre-filtering altogether, minimizes the possibility of information loss in these low
370 SNR recordings.

371 Another advantage of the NpD algorithm is that it is suitable for non-stationary background noise
372 since the upper bound to the spectral amplitude of background noise, above which an event is

detected, varies over both space and time; significant differences were observed in hourly noise characteristics between sensors 1km apart. The approach is also equally effective with non-parametric data i.e. an assumption of normality is not required. Details on the format of the input and output files for the NpD algorithm are provided in Supplementary Material, Section D.

Limitations of the NpD algorithm

The NpD algorithm is a powerful microseismicity detection tool but its output does not include accurate onset times for the detected events. Its accuracy depends on the duration of the individual time segments to which each recording is divided. For windows of duration 0.5 seconds, such as those used in this case study, it means that the onset time is within a 0.5 second frame centered around the estimated NpD time of the 'event'. For a more accurate determination of the onset time, the NpD would need to be combined with other existing automated picking algorithms, such as autoregressive techniques (Oye and Roth (2003); Kong (1997); Leonard and Kennett (1999)).

Comparison with other, commonly used detection approaches

In order to check the effectiveness of the NpD algorithm we compared its performance to that of the most commonly used detection algorithm, namely STA/LTA, and the algorithm suggested by Vaezi and van der Baan (2014).

For the comparison, we chose the same three hours (15/03/2016, hours 18:00-19:00 and 19:00-20:00 and 16/03/2016, hour 05:00-06:00 shown respectively at Figure 3, Figure 4 and Figure 5) from the GTS data set with varying background noise levels and with, and without, events. Table

4 shows the parameters used for each of the three detection methodologies used in the comparison. The detection thresholds in all methods are selected in such a way as to give the best balance between false positives and missed events for each algorithm. In Table 4, the *minimum event duration* parameter for the STA/LTA method is the minimal time length between the time of an event triggering and detriggering. The *minimum event separation* parameter specifies the minimal time length between the end of a previous event and the beginning of a new event. The STA and PSD window lengths were kept the same and equal to 0.5s to allow for a valid comparison of the algorithms. The same applies for the LTA window length and local window. The *consecutive events cleaning* parameter presumes that when the output peaks are consecutive within distances of 0.5s they correspond to the same event. All algorithms have been implemented in a multi-channel strategy in which events are detected only if they are detected by all vertical channels of each array.

Results are summarized in Figure 6 and Table 5. Figure 6 shows the filtered (bandstop 48-52 Hz to remove the AC effect) waveforms of the three hours examined previously, both as recorded from the North (a, c, & e) and the South Array (b, d & f). The vertical lines show the detection times obtained by the STA/LTA, PSD and NpD algorithms (see inset for details). From just visual inspection, it is noticeable that the STA/LTA detects very few events and the PSD algorithm detects many more events than the NpD. In Table 5 we can see the breakdown of these detected events to true and false positives. The ratios R1 and R2 were once again used to quantify the fraction of the total number of detected events that were visually observed (R1) and the fraction of the visually observed events that were detected (R2).

As seen from Table 5, the STA/LTA algorithm is outperformed by both the PSD picker and the NpD algorithm as its ability to detect events, when using unfiltered recordings is significantly

417 smaller (small values of the R2 ratio). The NpD algorithm also outperforms the PSD picker. For
418 those hours containing events, the NpD algorithm detects the same number of true events as the
419 PSD picker. However, the value of the R1 ratio is consistently higher for the NpD algorithm than
420 the PSD picker, indicating that the number of false positives from the NpD algorithm is
421 significantly smaller.

422 In the last tested hour, where there are no seismic events, the STA/LTA, PSD and NpD algorithms
423 detected 1, 1 and 3 at the North and 3, 15 and 7 false positives respectively. For this hour, the
424 STA/LTA is the best performing algorithm, with the smallest number of false positives. However,
425 the other two hours show that this is at the cost of missing large numbers of small events with
426 amplitudes close to noise level (low SNR).If a seismic array is deployed for decision-making
427 processes, such as an early-warning system for landslides, then visual validation of detected events
428 may be required by the operator (e.g. if road closure results in a long detour). This manual quality
429 control is a time-consuming procedure. The very low number of false positives that our NpD
430 algorithm detects, by comparison to the STA/LTA and PSD detection algorithms, ensures that
431 expensive operator time is minimized.

432

433 **CONCLUSIONS**

434 This work was motivated by the need for automatic detection of seismic signals from long,
435 continuous passive seismic recordings acquired by temporarily installed short-period seismic
436 arrays. The NpD algorithm is a powerful tool for microseismic event detection from noisy
437 recordings without the need for pre-filtering. This is a key advantage, as it does not require any a
438 priori assumptions on the background noise characteristics. The algorithm detects potential events

by calculating the energy contained within small individual time segments of a recording and comparing it to the energy contained within a longer surrounding time window. If the excess energy exceeds a given threshold criterion, which is determined dynamically based on the spatially and temporally varying background noise, then an event is detected. The efficiency of the NpD algorithm was successfully tested on a demanding data set. For event detection, it significantly outperforms the two STA/LTA and PSD algorithms tested, maximizing the number of detected events whilst minimizing the number of false positives.

DATA AND RESOURCES

Data and seismograms used in this study were collected as part of the LASMO project using Reftek instruments and are confidential until completion of the PhD.

For the NpD algorithm free accessible built-in functions from Matlab were used (MATLAB and Statistics Toolbox Release 2016a, The MathWorks, Inc., Natick, Massachusetts, United States.)

The Swiss Seismological Service catalogue database was searched using http://www.seismo.ethz.ch/en/earthquakes/switzerland/all-earthquakes/ (last accessed on November, 2017).

AKNOWLEDGEMENTS

This work is supported by RWM and is part of the collaborative LASMO (LArge Scale MOnitoring) program at Grimsel Test Site.

REFERENCES

Barnett, V. and T. Lewis (1994). *Outliers in statistical data*, Wiley, New York, **3**(1).

Bormann, P. (ed.) (2012). *New Manual of Seismological Observatory Practice (NMSOP-2), IASPEI*, GFZ German Research Centre for Geosciences, Potsdam.

Chambers, K., Kendall, J., Brandsberg-Dahl, S. and J. Rueda (2010). Testing the ability of surface arrays to monitor microseismic activity, *Geophys Prospect.* **58**(5) 821-830.

Das, I. and M.D. Zoback (2011). Long-period, long-duration seismic events during hydraulic fracture stimulation of a shale gas reservoir, *The Leading Edge.* **30**(7) 778-786.

Freiberger, W.F. (1963). An approximate method in signal detection. *Q J Mech Appl Math.* **20**(4) 373-378.

Gibbons, S.J. and F. Ringdal (2006). The detection of low magnitude seismic events using array-based waveform correlation, *Geophys J Int.* **165**(1) 149-166.

Goforth, T. and E. Herrin (1981). An automatic seismic signal detection algorithm based on the Walsh transform, *Bull. Seism. Soc. Am.* **71**(4) 1351-1360.

Helmstetter, A. and S. Garambois (2010). Seismic monitoring of Séchilienne rockslide (French Alps): Analysis of seismic signals and their correlation with rainfalls, *Journal of Geophysical Research. Earth Surface.* **115**(3).

Joswig, M. (1990). Pattern recognition for earthquake detection, *Bull. Seism. Soc. Am.* **80**(1) 170-186.

Joswig, M., Camelbeeck, T., Flick, T. and B. Ducarme (1992). System architecture of seismic networks and its implications to network automatization, *Cahiers Centre Europ. Geodyn. Seism.* **5** 75-84.

Kesler, S.B. and S. Haykin (1978). A comparison of the maximum entropy method and the periodogram method applied to the spectral analysis of computer-simulated radar clutter, *Canadian Electrical Engineering Journal*. ***3***(1) 11-16.

Kong, X. (1997). Forward and backward autoregressive modeling of EEG, in *Engineering in Medicine and Biology Society. Proceedings of the 19th Annual International Conference of the IEEE.* **3** 1215-1217.

Küperkoch, L., Meier, T., Lee, J., Friederich, W. and EGELADOS Working Group (2010). Automated determination of P-phase arrival times at regional and local distances using higher order statistics, *Geophys J Int.* **181**(2) 1159-1170.

Lee, W.H.K. and S.W. Stewart (1981). *Principles and applications of microearthquake networks,* Academic press, New York.

Leonard, M. and B.L.N. Kennett (1999). Multi-component autoregressive techniques for the analysis of seismograms, *Phys Earth Planet In.* **113**(1) 247-263.

Massey Jr, F.J. (1951). The Kolmogorov-Smirnov test for goodness of fit, *J Am Stat Assoc.* **46**(253) 68-78.

Maxwell, S. (2011). Microseismic hydraulic fracture imaging: The path toward optimizing shale gas production, *The Leading Edge*.

Nagra, 2017. *Large Scale Monitoring (LASMO) Introduction*. [online] Grimsel.com. Available at: http://www.grimsel.com/gts-phase-vi/lasmo/lasmo-introduction [Accessed 13 Oct. 2017].

Oye, V. and M. Roth (2003). Automated seismic event location for hydrocarbon reservoirs, *Comput Geosci.* **29**(7) 851-863.

Press, W.H. (2007). *Numerical recipes 3rd edition: The art of scientific computing*. Cambridge university press.

Pytharouli, S.I., Lunn, R.J., Shipton, Z.K., Kirkpatrick, J.D. and A.F. do Nascimento (2011). Microseismicity illuminates open fractures in the shallow crust, *Geophys Res Lett*, **38**(2).

Razali, N.M. and Y.B. Wah (2011). Power comparisons of Shapiro-Wilk, Kolmogorov-Smirnov, Lilliefors and Anderson-Darling tests, *Journal of statistical modeling and analytics.* **2**(1) 21-33.

Shensa, M. (1977). The deflection detector, its theory and evaluation on short-period seismic data, TR-77-03, Texas Instruments, Alexandria, Virginia.

Sun, Y. and M.G. Genton (2011). Functional boxplots, *J Comput Graph Stat.* **20**(2), 316-334.

Torgoev, A., Lamair, L., Torgoev, I. and H.B. Havenith (2013). A review of recent case studies of landslides investigated in the Tien Shan using microseismic and other geophysical methods. *Earthquake-Induced Landslides,* Springer, Berlin, Heidelberg, 285-294.

Trnkoczy, A. (1999). Understanding and parameter setting of STA/LTA trigger algorithm. *New Manual of Seismological Observatory Practice (NMSOP-2), IASPEI*, GFZ German Research Centre for Geosciences, Potsdam.

Vaezi, Y. and M. van der Baan (2014). Analysis of instrument self-noise and microseismic event detection using power spectral density estimates, *Geophys J Int.* **197**(2), 1076-1089.

519 Vaezi, Y. and M. van der Baan (2015). Comparison of the STA/LTA and power spectral density
520 methods for microseismic event detection, *Geophysical Supplements to the Monthly Notices of the*
521 *Royal Astronomical Society.* **203**(3), 1896-1908.

522 Welch, P. (1967). The use of fast Fourier transform for the estimation of power spectra: a method
523 based on time averaging over short, modified periodograms, *IEEE Trans Audio*
524 *Electroacoust.* **15**(2), 70-73.

525 Withers, M., Aster, R., Young, C., Beiriger, J., Harris, M., Moore, S. and J. Trujillo (1998). A
526 comparison of select trigger algorithms for automated global seismic phase and event
527 detection, *Bull. Seism. Soc. Am.* **88**(1) 95-106.

528 Zhou, R., Huang, L. and J. Rutledge (2010). Microseismic event location for monitoring CO2
529 injection using double-difference tomography, *The Leading Edge*.

530 Yfantis, G., Carvajal, H.E.M., Pytharouli, S. and R.J. Lunn (2014). Spectral Characteristics of
531 Landslide Induced Seismicity: Experimental Validation Based on the Use of an Up-Scaled Sheer
532 Box, in *AGU Fall Meeting Abstracts*.

533 Young, R. Paul, and C. D. Martin (1993). Potential role of acoustic emission / microseismicity
534 investigations in the site characterization and performance monitoring of nuclear waste
535 repositories, in *International journal of rock mechanics and mining sciences & geomechanics*
536 *abstracts.* Pergamon. **30**(7) 797-803.

FULL MAILING ADDRESS

M. Kinali, S. Pytharouli, R.J. Lunn, Z. Shipton, M. Stillings, R. Lord:

University of Strathclyde, Department of Civil and Environmental Engineering, University of Strathclyde, Glasgow, James Weir Building, Level 5, 75 Montrose Street, G1 1XJ, United Kingdom

S. Thompson:

Radioactive Waste Management, Building 587 , Curie Avenue, Harwell Oxford, Didcot, Oxfordshire, OX11 0RH, United Kingdom

TABLES

Table 1: Hour 1: Comparison of results for different values of the parameters of Noise PSD percentile and Local time window length.

Hour 1: 15/03/2016, 18:00 - 19:00													
	Actual no of events: 34	***North Array***											
	Noise PSD percentile:	***70***			***75***			***80***			***85***		
	Local window:	***150***	***300***	***450***	***150***	***300***	***450***	***150***	***300***	***450***	***150***	***300***	***450***
	Detected events:	*34*	*34*	*34*	*37*	*37*	*37*	*38*	*37*	*36*	*37*	*37*	*36*
	True positives:	*31*	*30*	*29*	*32*	*32*	*32*	*32*	*32*	*32*	*32*	*32*	*32*
	R1	*91%*	*88%*	*85%*	*86%*	*86%*	*86%*	*84%*	*86%*	*89%*	*86%*	*86%*	*89%*
	R2	*91%*	*88%*	*85%*	*94%*	*94%*	*94%*	*94%*	*94%*	*94%*	*94%*	*94%*	*94%*
	Actual no of events: 27	***South Array***											
	Noise PSD percentile:	***70***			***75***			***80***			***85***		
	Local window:	***150***	***300***	***450***	***150***	***300***	***450***	***150***	***300***	***450***	***150***	***300***	***450***
	Detected events:	*28*	*29*	*28*	*28*	*29*	*28*	*28*	*29*	*28*	*27*	*29*	*29*
	True positives:	*25*	*25*	*25*	*24*	*25*	*25*	*25*	*25*	*25*	*25*	*25*	*25*
	R1	*89%*	*86%*	*89%*	*86%*	*86%*	*89%*	*89%*	*86%*	*89%*	*93%*	*86%*	*86%*
	R2	*93%*	*93%*	*93%*	*89%*	*93%*	*93%*	*93%*	*93%*	*93%*	*93%*	*93%*	*93%*

Table 2: Hour 2: Comparison of results for different values of the parameters of Noise PSD percentile and Local time window length.

Hour 2: 15/03/2016, 19:00 - 20:00													
	Actual no of events: 18	**North Array**											
	Noise PSD percentile:	**70**			**75**			**80**			**85**		
	Local window:	**150**	**300**	**450**	**150**	**300**	**450**	**150**	**300**	**450**	**150**	**300**	**450**
	Detected events:	30	30	31	30	31	32	29	32	31	28	35	32
	True positives:	18	18	18	18	18	18	18	18	18	18	18	18
	R1	60%	60%	58%	60%	58%	56%	62%	56%	58%	64%	51%	56%
	R2	100%	100%	100%	100%	100%	100%	100%	100%	100%	100%	100%	100%
	Actual no of events: 19	**South Array**											
	Noise PSD percentile:	**70**			**75**			**80**			**85**		
	Local window:	**150**	**300**	**450**	**150**	**300**	**450**	**150**	**300**	**450**	**150**	**300**	**450**
	Detected events:	20	24	25	20	24	29	20	28	31	23	32	34
	True positives:	16	16	16	16	16	16	16	16	16	16	16	16
	R1	80%	67%	64%	80%	67%	55%	80%	57%	52%	70%	50%	47%
	R2	84%	84%	84%	84%	84%	84%	84%	84%	84%	84%	84%	84%

Table 3: Hour 3: Comparison of results for different values of the parameters of Noise PSD percentile and Local time window length.

Hour 3: 16/03/2016, 05:00 - 06:00													
	Actual no of events: 0	**North Array**											
	Noise PSD percentile:	**70**			**75**			**80**			**85**		
	Local window:	**150**	**300**	**450**	**150**	**300**	**450**	**150**	**300**	**450**	**150**	**300**	**450**
	Detected events:	3	2	2	3	3	3	5	3	3	6	5	3
	True positives:	0											
	Actual no of events: 0	**South Array**											
	Noise PSD percentile:	**70**			**75**			**80**			**85**		
	Local window:	**150**	**300**	**450**	**150**	**300**	**450**	**150**	**300**	**450**	**150**	**300**	**450**
	Detected events:	8	7	9	8	7	12	8	9	15	9	11	15
	True positives:	0											

556 Table 4: The parameters used for the STA/LTA, PSD technique and NpD methods.

STA/LTA parameters		***PSD technique parameters***		***NpD parameters***	
STA window length	0.5s	PSD window length	0.5s	Individual time segment duration	0.5s
Minimum event duration	0.005s	Window overlap	50%	Noise PSD	75^{th}
Minimum event separation	0.5s	Minimum event separation	0.5s	Consecutive events cleaning	0.5s
LTA window length	5mins	_		Local window	5mins
STA/LTA detection threshold	2.5	PSD detection threshold	0.50	Dynamic detection threshold	Q3+0.5IQR

557

558 Table 5: Summary of detections using the STA/LTA, the PSD and the NpD algorithms for hours

559 1, 2 and 3, for both North and South arrays.

560

		STA/LTA algorithm	*PSD Picker*	*NpD algorithm*
Hour 1: 15/03/2016, 18:00 - 19:00	***Actual no of events: 34***		***North Array***	
	Detected events:	*4*	*123*	*37*
	True positives:	*4*	*32*	*32*
	R1	*100%*	*26%*	*86%*
	R2	*12%*	*94%*	*94%*
	Actual no of events: 27		***South Array***	
	Detected events:	*3*	*102*	*29*
	True positives:	*3*	*24*	*25*
	R1	*100%*	*24%*	*86%*
	R2	*11%*	*89%*	*93%*
Hour 2: 15/03/2016, 19:00 - 20:00	***Actual no of events: 18***		***North Array***	
	Detected events:	*12*	*97*	*31*
	True positives:	*3*	*18*	*18*
	R1	*25%*	*19%*	*58%*
	R2	*17%*	*100%*	*100%*
	Actual no of events: 19		***South Array***	
	Detected events:	*13*	*140*	*24*
	True positives:	*1*	*16*	*16*
	R1	*8%*	*11%*	*67%*
	R2	*3%*	*47%*	*84%*
Hour 3: 15/03/2016, 05:00 - 06:00	***Actual no of events: 0***		***North Array***	
	Detected events:	*1*	*1*	*3*
	True positives:	*0*	*0*	*0*
	Actual no of events: 0		***South Array***	
	Detected events:	*3*	*15*	*7*
	True positives:	*0*	*0*	*0*

561

FIGURES

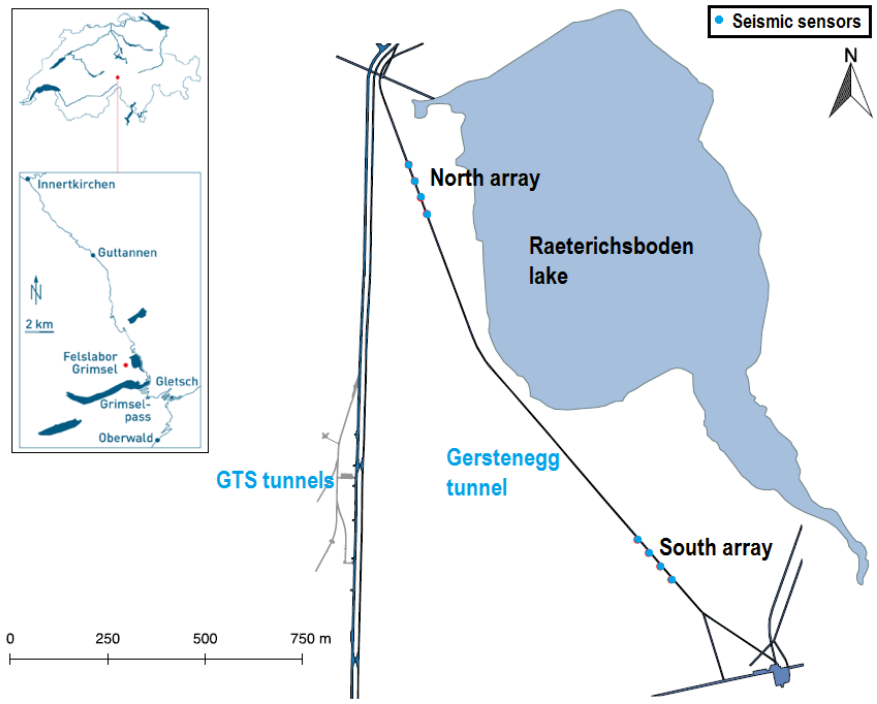

Figure 1: Plan view of the locations of two surface microseismic arrays deployed at GTS. Two surface arrays, consisting of four sensors each, were deployed along the Gerstenegg tunnel, close to the GTS tunnels. The elevation of all tunnels is lower to the water surface in Lake Raeterichsboden. Inset: Location map of GTS (from http://www.nagra.ch/en/grimselrocklaboratory.htm).

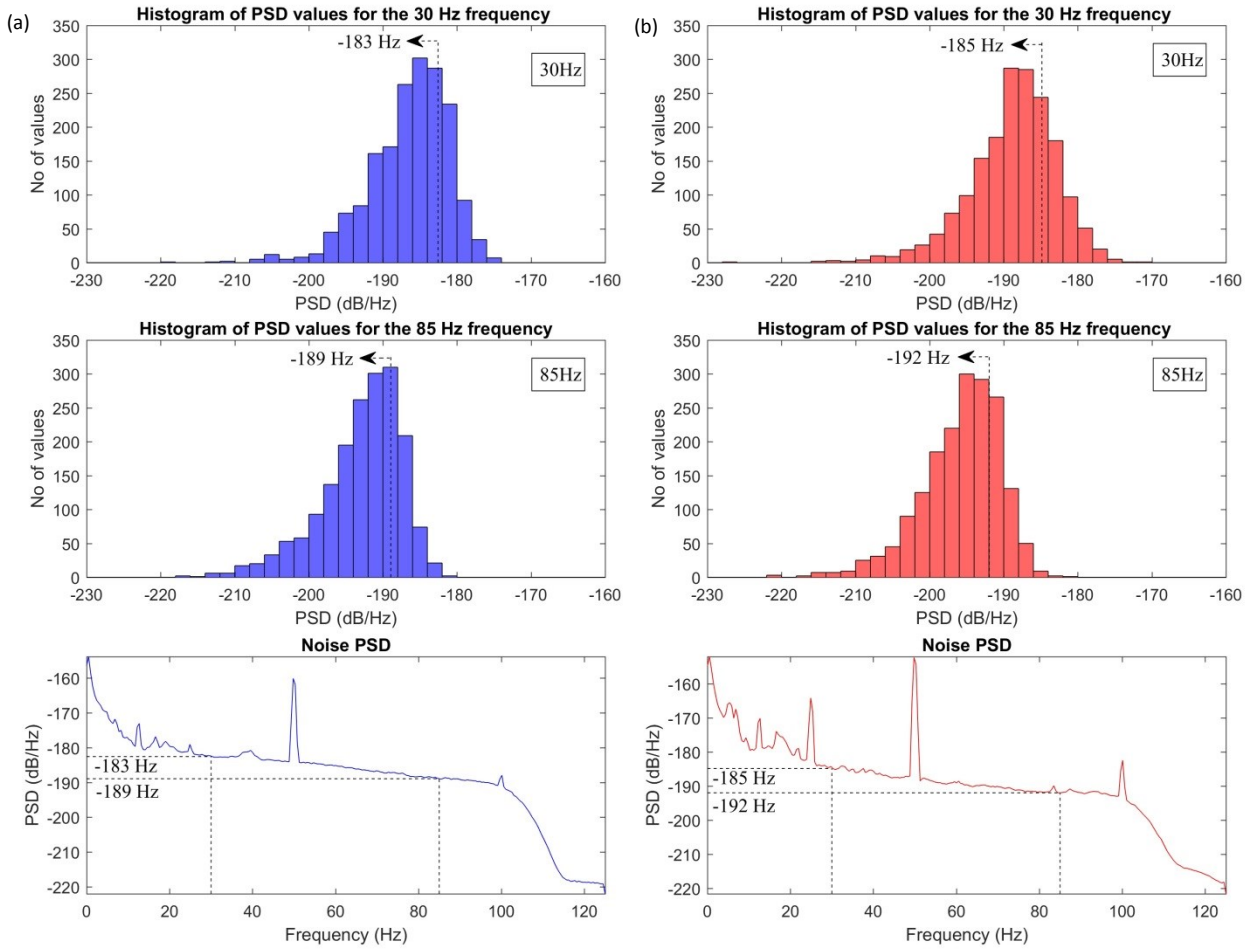

570

571 Figure 2: Calculation of the Noise PSD for one hour of data recorded by the vertical component
572 of the 3-component seismometer of (a) the North and (b) the South array. The histograms of the
573 PSD values at frequencies 30 Hz and 85 Hz and the value of a characteristic upper bound (here the
574 75th percentile) are shown as an example. These values are then used as the Noise PSD values at
575 30 Hz and 85 Hz frequencies, respectively. The values of the characteristic upper bound for all

frequencies constitute the Noise PSD (bottom plots in (a) and (b)). All histograms are for data from the same day and hour.

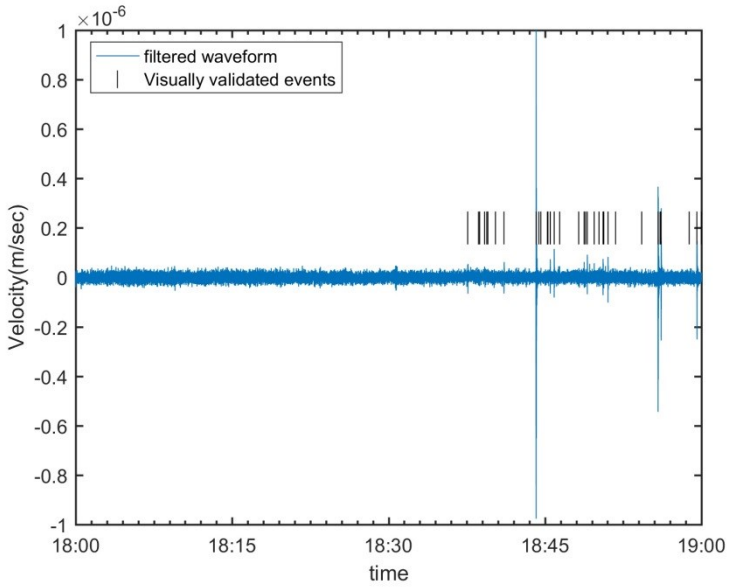

Figure 3: Hour 1: Filtered waveform and visually identified events are shown with vertical lines.

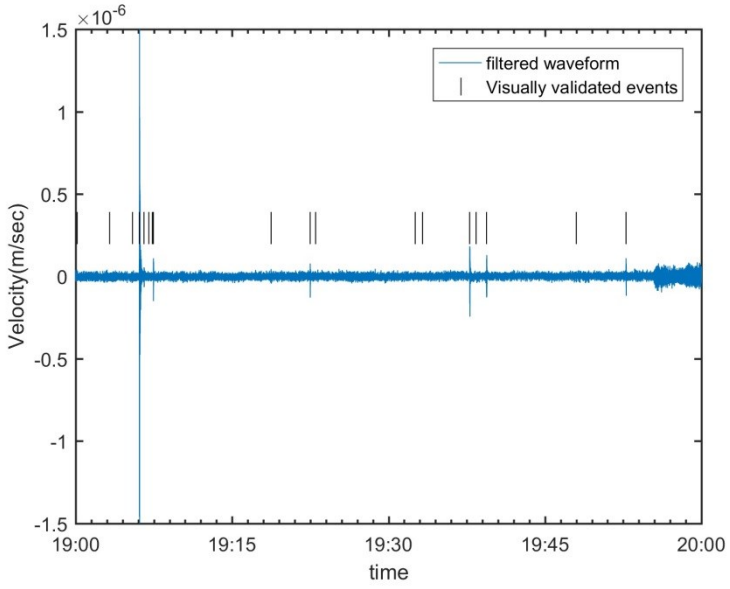

Figure 4: Hour 2: Filtered waveform and visually identified events are shown with vertical lines.

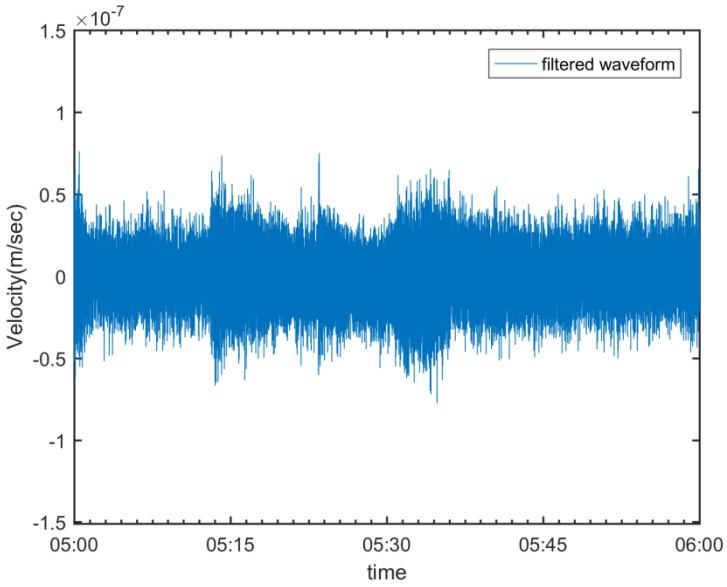

582

583 Figure 5: Hour 3: Filtered waveform. Hour with no visually identified events.

584

585

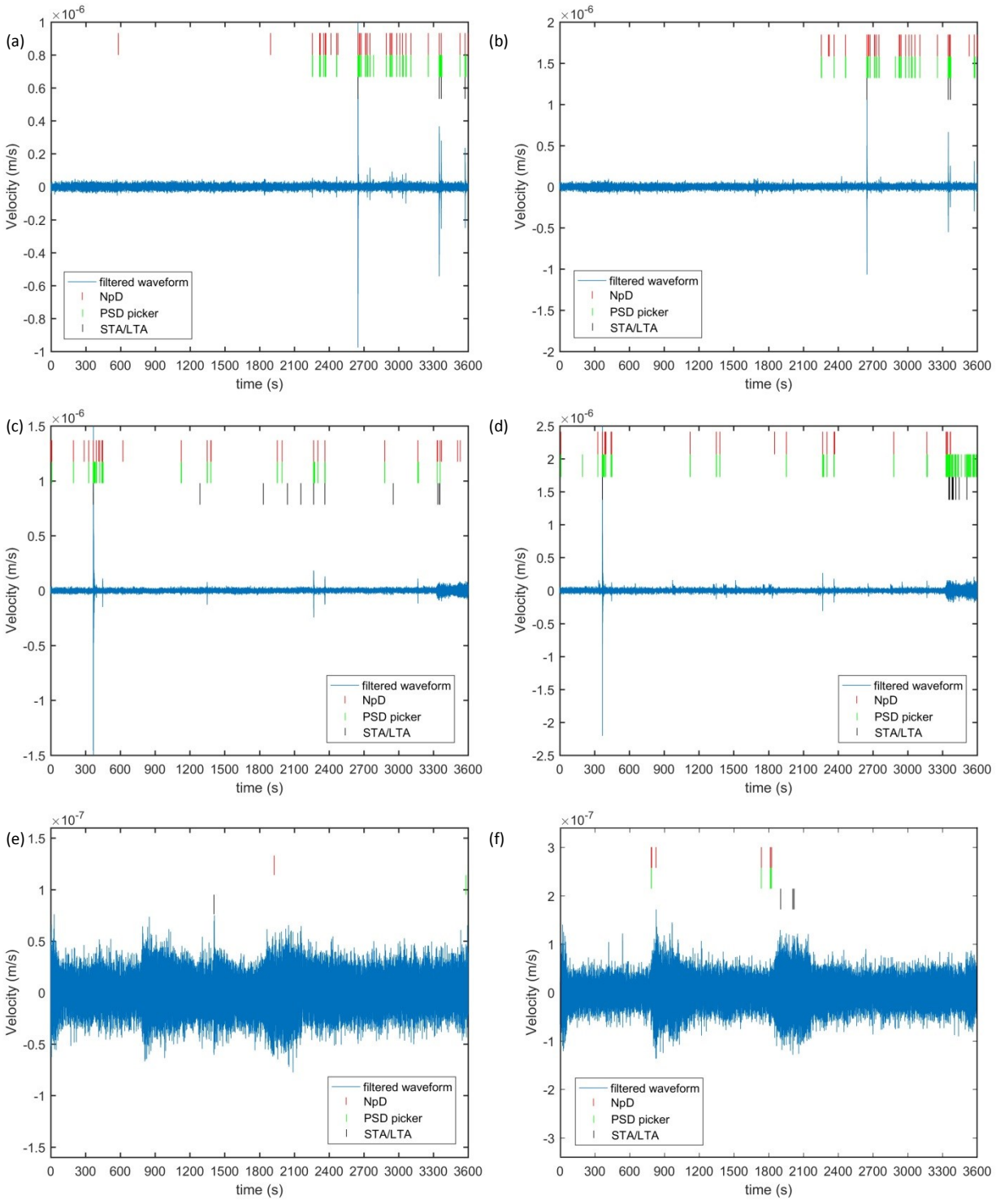

Figure 6: Velocity vs time for the filtered waveforms of (a & b) 15/03/2016, 18:00-19:00, (c & d) 15/03/2016, 19:00-20:00, and (e & f) 16/03/2016, 05:00-06:00 as recorded from the North and

589 South array respectively. With vertical lines the events detected by the NpD algorithm, the PSD
590 technique and the STA/LTA algorithm are noted.

591

DETECTION OF WEAK SEISMIC SIGNALS IN NOISY ENVIRONMENTS FROM UNFILTERED, CONTINUOUS PASSIVE SEISMIC RECORDINGS - SUPPLEMENTARY MATERIAL

M. Kinali, S. Pytharouli, R.J. Lunn, Z. K. Shipton, M. Stillings, R. Lord and S. Thompson

SUPPLEMENTARY MATERIAL

A brief review of the automatic seismic signals detection methods is given in Section A. In particular time domain methods are presented, such as STA/LTA (Bormann, 2012) and Stewart (1977) method; frequency domain methods such as those proposed by Freiberger (1963), Goforth and Herrin (1981), Michael et al. (1982), Vaezi and Van de Baan (2014, 2015) and Shensa (1977); and time-frequency domain methods such as Joswig (1990), Ching et al. (2004), Sifuzzaman et al. (2009) and Anant and Dowla (1997). In Section B, Welch's (1967) modified periodogram method is discussed, along with its limitations.

In Section C, the statistical analysis presented in the paper is explained in detail, in particular the temporal and spatial comparison among non-normal distributions of random, independent PSD observations. Section D is describing the input and output variables of the NpD algorithm which is going to be distributed as an open-source detection algorithm.

REVIEW OF AUTOMATIC SEISMIC EVENT DETECTION ALGORITHMS

Automatic detection in the time domain

The most widely used event detection algorithm at present is the STA/LTA (Bormann, 2012) which operates in the time-domain. The ratio of two moving averages STA/LTA is computed continuously at each time t for recorded data x_t:

$$STA_t = \frac{1}{N_S}\sum_{n=t}^{t+N_S} y_n \ , \qquad \text{(eq. S2)}$$

and

$$LTA_t = \frac{1}{N_L}\sum_{n=t}^{t+N_L} y_n . \qquad \text{(eq. S3)}$$

where STA is the N_S-point Short-Term Average, LTA is the N_L-point Long-Term Average and the parameter y_t denotes a characteristic function (CF) $y_t = g(x_t)$. The characteristic function CF is chosen so that it enhances any signal changes in the time-series; common CF choices include energy (x_t^2) (McEvilly and Majer, 1982), absolute value ($|x_t|$) (Swindell and Snell, 1977) and the envelope function ($\sqrt{x_t^2 + \bar{x}_t^2}$, where $\bar{x}$ is the Hilbert transform) (Earle and Shearer, 1994), or even higher-order statistics where skewness and kurtosis are calculated in the sliding windows (Saragiotis et al., 2002; Küperkoch et al., 2010). The raw data are demeaned and then the ratio STA/LTA is compared to a user-selected threshold: when the ratio exceeds the user-selected threshold, an event is detected. The end time of the event is defined by the time when the ratio falls below a detrigger threshold (also chosen by the user). N_s should be chosen approximately equal to the dominant period of the events the algorithm aims to trigger. LTA is a measure of background noise variations, so N_L should be set to some value longer than the period of the lowest frequency

seismic signal of interest. The STA, LTA windows are usually chosen as non-overlapping (Trnkoczy, 2002).

A different approach was suggested by Stewart (1977). This method uses a high-pass non-linear filtering process, to determine whether a seismometer is operating within acceptable limits of noise before its data are accepted to be used. If accepted, the algorithm sets some requirements for detection and tentative confirmation in the time domain, i.e. setting different lower bounds for the triggering threshold, the SNR; the number of times the waveform exceeds the triggering threshold; the consecutive time the waveform stays within the threshold; and the maximum amplitude of the waveform once the signal is detected.

Model-oriented algorithms are also popular, such as the Oye and Roth (2003) or Akram and Eaton (2012) autoregressive (AR) techniques. Based on the Akaike Information Criterion (AIC), they developed procedures of fitting a locally stationary autoregressive model to seismograms. The AIC criterion, computed using the estimated model order, provides a measure of the model fit, and an optimal separation of the two stationary time series (noise and signal) is indicated by the time index associated with the minimum value of AIC (Tronicke, 2007).

Automatic detection in the frequency domain

Most algorithms in the frequency domain use Fourier transforms. One of the first mathematically based signal detectors was the one proposed by Freiberger (1963) who developed the theory of maximum likelihood by applying an approximate comparison of spectral densities, based on the Toeplitz approximation forms, for the detection of Gaussian signals in Gaussian noise.

Goforth and Herrin (1981), in order to overcome the challenge of a varying non-normal background noise, developed an automatic seismic signal detector based on the Walsh transform, which is a series of rectangular waveforms with amplitudes of +1 or -1, instead of the sines and cosines of Fourier. Once the data are filtered in the time domain, segmented in overlapping windows and transformed, the Walsh coefficients are assigned a weight such that the noise spectrum is whitened and the expected signal is isolated. The values of the weights need to be chosen by the analyst, after manual inspection of the appropriate noise segments. At each time window, the current sum of the absolute values of the weighted Walsh coefficients is compared to a threshold,

$$Threshold = V_{50} + K(V_{75} - V_{50}), \quad \text{(eq. S4)}$$

where V_{50} is the median of the distribution of previous 512 values, V_{75} is the 75th percentile of the distribution of previous values, and K is the arbitrary constant set by operator. If the current value exceeds the threshold, it results in a signal detection; if not, the current sum is ranked among the previous number of predefined values and the oldest sum is discarded.

Michael et al. (1982) modified the Goforth and Herrin approach to develop a real-time event detection and recording system for the MIT Seismic Network. Their algorithm uses the power spectrum to remove the effects of phase shifts and instead of the Walsh coefficients (energy spectrum) they use power Walsh coefficients (i.e. the Walsh coefficients are squared and each pair is summed). They also add a minimum duration that the coefficients need to be above threshold; an event termination criterion; and accept events only if they are correlated by at least three stations.

Vaezi and Van de Baan (2014, 2015) developed an algorithm for the detection of induced microseismicity during hydrofracturing. They compared the moving average PSDs of small segments of their data record to the averaged background noise PSD of quiet segments of their data record, resulting in the picking of all signals that stand out in a statistical sense from background noise. The outcome of this comparison, i.e. the normalized misfit $u_t(f)$, is calculated by the following equation (eq.S4) and for a clearer depiction of the events, only the positive values are kept:

$$u_t(f) = \begin{cases} \frac{PSD_n^t(f) - \overline{PSD}(f)}{std(f)}, if\ u_t(f) > 1 \\ 0 \quad , otherwise \end{cases}, \qquad \text{(eq. S5)}$$

where $std(f)$ is the standard deviation at frequency f computed from the PSDs of the noise segment $PSD'_m(f)$, $PSD_n^t(f)$ are the PSDs of small segments of the original data x(t) estimated (eq.S5), using rolling (overlapping) windows of predetermined length L, and $\overline{PSD}(f)$ is the total average PSD of the quiet sections of the data x'(t) (eq.S6). To isolate only the quiet sections they discarded all the absolute amplitudes greater than a multiple of the original record's root-mean-square (RMS) amplitude.

The individual moving average PSDs are estimated using Welch's modified periodogram method as follows:

$$PSD_n^t(f) = \begin{cases} \frac{a\left|\sum_{l=1}^{L} x_n(t_l)\omega(t_l)e^{-j2\pi fl}\right|^2}{f_s LU} \quad if\ f = 0, f_{Nyq} \\ \frac{2a\left|\sum_{l=1}^{L} x_n(t_l)\omega(t_l)e^{-j2\pi fl}\right|^2}{f_s LU} \quad if\ 0 < f < f_{Nyq} \end{cases}, \quad \text{n = 1, 2, …, N} \qquad \text{(eq. S6)}$$

where a is a scale factor that accounts for variance reduction which depends on the type of the taper w, f_{Nyq} is the Nyquist frequency in Hz, fs is the sampling frequency in Hz, $j = \sqrt{-1}$ and U is

690 the window normalization constant that ensures the modified periodograms are asymptotically
691 unbiased and is given by: $U = \frac{1}{L}\sum_{i=1}^{L} \omega(t_i)^2$.

692 The average PSD estimate is calculated by averaging the PSD estimates of the quiet data record:

693 $$\overline{PSD}(f) = \frac{1}{M}\sum_{i=1}^{M} PSD'_m(f), \quad \text{(eq. S7)}$$

694 where $PSD'_m(f)$ denotes the PSD estimate of the mth noise segment as a function of frequency f
695 and is given by eq.S5 where instead of the original data x(t) we are now using the quiet data record
696 x'(t).

697 The triggering criterion can either be the summation of the positive misfits ($u_t(f)$) over the total
698 number of frequencies and normalized by division with the standard deviation, or the summation
699 of the squared positive misfits over the total number of frequencies normalized by division with
700 the standard deviation. When the triggering criterion exceeds a user-selected threshold an event is
701 declared.

702 Shensa (1977) had developed a methodology to adapt to a dynamic noise environment with a
703 variety of (weak) signals with widely different spectra. He computed the PSDs of small segments
704 of the data and depending on the relation between noise and signal he developed 3 algorithms: (a)
705 the average power detector, for signals that exceed noise uniformly over a relatively broad
706 frequency index range when both noise and signal are stable; (b) the maximum deflection detector,
707 for signals that exceed noise over at least one narrow frequency band; and (c) the average
708 deflection detector, for signals that exceed background noise uniformly over a relatively wide
709 frequency index range when both signal and noise are unstable. The relevant detectors are formed
710 accordingly:

$$Det_a = \frac{\frac{1}{N}\sum_{k=n_1}^{n_2} PSD_i(k) - \mu}{\sigma}, N = n_2 - n_1, \quad \text{(eq. S8)}$$

$$Det_b = \max\left[\frac{P_i(k)-\mu(k)}{\sigma(k)}\ (k=0), \frac{P_i(k)-\mu(k)}{\sigma(k)}\ (k=1), \ldots, \frac{P_i(k)-\mu(k)}{\sigma(k)}\ (k=N)\right], \quad \text{(eq. S9)}$$

$$Det_c = \frac{1}{N}\sum_{k=n_1}^{n_2} \frac{P_i(k)-\mu(k)}{\sigma(k)}\ , N = n_2 - n_1, \quad \text{(eq. S10)}$$

where index range $n_1 \leq k \leq n_2$, μ and σ the mean and standard deviation, respectively. The parameters μ and σ must be estimated from noise-only data sections (i.e. no signal present).

Automatic detection in the time-frequency domain

Algorithms that work in the time-frequency domain are also common. Joswig (1990) proposed a pattern recognition technique using characteristic event features in spectrograms. His algorithm defines a knowledge base of images of the typical earthquakes and noise bursts in the time-frequency domain, using Fourier transforms, each of which is defined by a matrix and a scaling factor (to account for magnitude differences). The sonogram-detector matches patterns for the events that are above a user-defined set of thresholds and provides one message per detected event stating the detection time, the maximum pattern fit and maximum amplitude of the detected event.

Another pattern recognition technique was proposed by Bodenstain and Praetorius (1977) aimed at the automatic detection of electroencephalogram signals (0.5 – 30Hz signals). According to their research, the data record can be segmented into elementary patterns (e.g. seismic signals and transients) using linear predictive filtering, leading to the extraction of features (power spectra and

730 the signal's time structure) which in turn can be combined (clustering procedures, classification)
731 so that they represent the seismic signal as a whole.

732 During the last years, Wavelet transforms have increasingly been preferred over Fourier
733 transforms. The main reason being the simultaneous time- and frequency-domain localization of
734 the wavelets, in contrast to the only frequency-domain localization of the standard Fourier
735 transform, or the frequency-time resolution trade-off of the Short-time Fourier transform which
736 depends on the width of the window function used (Ching et al., 2004; Sifuzzaman et al., 2009).
737 Anant and Dowla (1997) use polarization and amplitude information contained in the wavelet
738 transform coefficients of the signals to construct "locator" functions that identify the P and S
739 arrivals. High-pass and low-pass filters are used (wavelet and scaling filters respectively) which
740 must belong to a perfect reconstruction filter bank.

741

742 **THE WELCH'S MODIFIED PERIODOGRAM METHOD (1967)**

743 Welch's method consists of breaking the time series into, usually overlapping, segments,
744 computing a modified periodogram of each of these segments, and then averaging their PSD
745 estimates (eq.S5). Each segment represents approximately uncorrelated estimates of the true PSD
746 and the averaging reduces the variance of the estimate as compared to the estimate of a single
747 periodogram for the entire time series. The segments are typically multiplied by a window
748 function, such as a Hamming or a Hann window, resulting into the estimation of modified
749 periodograms. Windowing suppresses side-lobe spectral leakage and reduces the bias of the
750 spectral estimates. The taper used in this study is Hann window which is one of the most commonly

used for its very good spectral leakage properties (Park et al., 1987). The coefficients of a Hamming and a Hann window can be generated from the following equations respectively:

$$w(n) = 0.54 - 0.46\cos\left(2\pi\frac{n}{N}\right), \quad \text{(eq. S11)}$$

$$w(n) = 0.5(1 - \cos\left(2\pi\frac{n}{N}\right)), \quad \text{(eq. S12)}$$

where $0 \leq n \leq N$ and window length = N+1

The loss of information at the limits of each segment caused by the windowing is prevented with the use of overlap at the adjacent segments. However, overlap introduces also redundant information. The combined use of short data records and nonrectangular windows results in reduced resolution of the estimator. This trade-off between variance reduction and resolution cannot be avoided (Park et al., 1987) and this is the shortcoming of this method. It lies with the analyst to decide on what is the feature they want to have the greatest accuracy at and choose the respective parameters to achieve that.

The one-sided PSD is calculated at discrete equally spaced frequency values within the range 0 to f_{Nyq}, where f_{Nyq} is the Nyquist frequency (equal to half the sampling rate f_s). The PSD spectrum is plotted as a continuous function, assuming a linear change between the calculated values at each frequency. A high peak in the PSD is interpreted as high energy in the signal at that frequency.

STATISTICAL CHARACTERIZATION OF THE BACKGROUND NOISE

770 To statistically compare the non-normal distributions of random, independent PSD observations
771 of size $f_{Nyq,}$ we perform two independent sub-analyses: temporal and spatial. The temporal subpart
772 is composed of upper Noise envelopes of different hours for one of the seismometers, while the
773 spatial subpart comprises of upper Noise envelopes of different seismometers. Examples of the
774 PSDs plotted against the frequency range used for the temporal and spatial comparison are
775 presented in Figure S1. Just by visual observation of the Figure S1a it is evident that the noise is
776 different not only for different days but also for different hours within the same day. As it concerns
777 the spatial variation, Figure S1b shows the PSD spectrum of one hour of data obtained from the
778 seismometers of the North and South array. It can be seen that the spectra differ even for the
779 seismometers of the same array (distances between adjacent sensors less than 50 m).

780 For the temporal subpart we perform an observational study for 4 independent time intervals (TI)
781 (TI 1:4, see inset of Figure S1a). TI1 is the Noise envelope for hour 15:00-16:00 on the 04/11/2014
782 (working hour), TI2 for hour 21:00-22:00 on the same day (out of working hours, diurnal
783 variation), TI3 for hour 15:00-16:00 (same as TI1) on the 05/11/2014 (monthly variation) and TI4
784 for hour 15:00-16:00 (again same hour) on the 16/05/2015 (annual variation). For the spatial
785 subpart a cross-sectional study for 3 independent TIs (TI 1:3, see inset of Figure S1b). TI1 is the
786 Noise envelope for a vertical seismometer of the North array for hour 15:00-16:00 on the
787 04/11/2014, TI2 is for a vertical seismometer of the South array (temporal variation between
788 arrays) while TI3 is the Noise envelope for the 3D vertical seismometer of the South array
789 (temporal variation between different sensors within one array).

790 At both temporal and spatial analysis subparts the Kruskal-Wallis test (Chan and Walmsley, 1997)
791 was applied. In both the temporal and spatial analysis the [medians (Q_1, Q_3)] were found to be

792 significantly different between TIs at the level of significance 0.05 (see Table S1 for the descriptive
793 statistics of each subpart).

794

795

796 **THE NPD ALGORITHM: INPUT AND OUTPUT FILES**

797 The NpD algorithm is going to be distributed as an open-source detection algorithm. The algorithm
798 steps (Step 1 and 2) have been automatized in the form of a code that runs in Matlab environment.
799 The raw seismic data are converted from ASCII format to MATLAB files using simple algorithms.
800 In this step the files are named: sensor_year_DOY_hour_min_sec_μs_ channel, where sensor can
801 be either LOC1, LOC2 or BH, DOY is the day of the year, the μsec have an accuracy of four digits
802 and channel can be CH1:6. Then the mat files are pre-processed before fed into the algorithm: the
803 counts are converted to ground velocity within the passband. Faulty files are dismissed (e.g. files
804 that due to electrical malfunction of the sensors recorded some minutes instead of a full hour data
805 record) during this step. The data are filtered with just a band-stop recursive Butterworth filter at
806 48-52Hz to remove the mains electromagnetic interference which is prevalent. No further filtering
807 has been applied. The mat files are also demeaned and fed into the algorithm as structure arrays.
808 Each structure array contains four fields: data (900000 data points), date (character array in the
809 form of 'dd-mmm-yyyy HH:MM:SS.mmmm' which indicates the beginning of the file), sensor
810 (e.g. 'LOC2') and channel (e.g. 'CH1').

811 The output of the code contains the variable 'FinalRslts' which is a structure array with 3 fields:
812 names (character array in the form of 'DOY_HH'), times (the times from the beginning of the hour
813 the potential events are detected, in sec), timesForXcel (the times from the beginning of the hour

814 the potential events are detected, in MM:SS:mmm). The variable 'listingTotal' is another useful
815 output variable of the code listing the full names of the files checked from the code. The output
816 variables 'Step1_all_values' contains two column cells: the second column encloses the file
817 checked while the first the values of misfits and corresponding times of all data points during the
818 first step of the algorithm. The output variables 'Step1_above_threshold' follows the logic of
819 'Step1_all_values' only this time the first column cells enclose the values of misfits and
820 corresponding times of only the data points that successfully passed the first step of the algorithm.
821 The output variable 'PredictedEventsIndivChannel' follows the previous logic and contains all
822 values of misfits and corresponding times of only the data points that successfully passed the
823 second step of the algorithm. This variable is different from the 'FinalRslts' because the former
824 refers to individual channels (the voting scheme has not yet been applied), neither has the
825 consecutive events cleaning.

826 **REFERENCES**

827 Akram, J. and D. Eaton (2012). Adaptive microseismic event detection and automatic time
828 picking, in *2012 CSEG Annual Convention* **15**.

829 Anant, K.S. and F.U. Dowla (1997). Wavelet transform methods for phase identification in three-
830 component seismograms, *Bull. Seism. Soc. Am.* **87**(6) 1598-1612.

831 Bodenstein, G. and H.M. Praetorius (1977). Feature extraction from the electroencephalogram by
832 adaptive segmentation, *Proceedings of the IEEE* **65**(5) 642-652.

833 Bormann, P. (ed.) (2012). *New Manual of Seismological Observatory Practice (NMSOP-2),*
834 *IASPEI*, GFZ German Research Centre for Geosciences, Potsdam.

835 Chan, Y. and R.P. Walmsley (1997). Learning and understanding the Kruskal-Wallis one-way
836 analysis-of-variance-by-ranks test for differences among three or more independent groups, *Phys*
837 *Ther.* **77**(12) 1755-1761.

838 Ching, J., To, A.C. and S.D. Glaser (2004). Microseismic source deconvolution: Wiener filter
839 versus minimax, Fourier versus wavelets, and linear versus nonlinear, *J Acoust Soc Am.* **115**(6)
840 3048-3058.

841 Earle, P.S. and P.M. Shearer (1994). Characterization of global seismograms using an automatic-
842 picking algorithm, *Bull. Seism. Soc. Am.* **84**(2) 366-376.

843 Freiberger, W.F. (1963). An approximate method in signal detection. *Q J Mech Appl Math.* **20**(4)
844 373-378.

845 Goforth, T. and E. Herrin (1981). An automatic seismic signal detection algorithm based on the
846 Walsh transform, *Bull. Seism. Soc. Am.* **71**(4) 1351-1360.

847 Joswig, M. (1990). Pattern recognition for earthquake detection, *Bull. Seism. Soc. Am.* **80**(1) 170-
848 186.

849 Küperkoch, L., Meier, T., Lee, J., Friederich, W. and EGELADOS Working Group (2010).
850 Automated determination of P-phase arrival times at regional and local distances using higher
851 order statistics, *Geophys J Int.* **181**(2) 1159-1170.

852 McEvilly, T.V. and E.L. Majer (1982). ASP: An automated seismic processor for microearthquake
853 networks, *Bull. Seism. Soc. Am.* **72**(1) 303-325.

854 Michael, A.J., Gildea, S.P. and J.J. Pulli (1982). A real-time digital seismic event detection and
855 recording system for network applications, *Bull. Seism. Soc. Am.* **72**(6A) 2339-2348.

856 Oye, V. and M. Roth (2003). Automated seismic event location for hydrocarbon reservoirs,
857 *Comput Geosci* **29** 851–863, doi: 10 .1016/S0098-3004(03)00088-8.

858 Park, J., Lindberg, C.R. and F.L. Vernon III (1987). Multitaper spectral analysis of high-frequency
859 seismograms, *J. Geophys. Res.* **92** 12675–12684.

860 Saragiotis, C.D., Hadjileontiadis, L.J. and S.M. Panas (2002). PAI-S/K: A robust automatic
861 seismic P phase arrival identification scheme, *IEEE Trans Geosci Rem Sens.* **40**(6) 1395-1404.

862 Shensa, M. (1977). The deflection detector, its theory and evaluation on short-period seismic data,
863 TR-77-03, Texas Instruments, Alexandria, Virginia.

864 Sifuzzaman, M., Islam, M.R. and M.Z. Ali (2009). Application of wavelet transform and its
865 advantages compared to Fourier transform, *Journal of Physical Sciences.* **13** 121-134**.**

866 Stewart, S.W. (1977). Real-time detection and location of local seismic events in central
867 California, *Bull. Seism. Soc. Am.* **67**(2) 433-452.

868 Swindell, W.H. and N.S. Snell (1977). Station processor automatic signal detection system, phase
869 I: Final report, station processor software development. *Texas Instruments Final Report No. ALEX*
870 *(01)-FR-77*, *1*.

871 Vaezi, Y. and M. van der Baan (2014). Analysis of instrument self-noise and microseismic event
872 detection using power spectral density estimates, *Geophys J Int.* **197**(2), 1076-1089.

873 Vaezi, Y. and M. van der Baan (2015). Comparison of the STA/LTA and power spectral density
874 methods for microseismic event detection, *Geophysical Supplements to the Monthly Notices of the*
875 *Royal Astronomical Society.* **203**(3), 1896-1908.

876 Tronicke, J. (2007). The influence of high frequency uncorrelated noise on first-break arrival times
877 and crosshole traveltime tomography, *J Environ Eng Geophys.* **12**(2), 173-184.

878 Trnkoczy, A. (1999). Understanding and parameter setting of STA/LTA trigger algorithm. *New*
879 *Manual of Seismological Observatory Practice*, *2*.

880

881 **LIST OF TABLE CAPTIONS**

882 Table S1: Descriptive statistics for temporal and spatial subparts of nonparametric analysis

883

884 **LIST OF FIGURE CAPTIONS**

885 Figure S1: (a) Temporal variation of background noise and (b) spatial variation of background
886 noise

887